Journal of Superconductivity and Novel Magnetism (2020) 33:2829–2836
https://doi.org/10.1007/s10948-020-05538-7

ORIGINAL PAPER

Structural and Magnetic Properties of the New $SrLa_2FeCuSbO_9$ Perovskite Phase

Noureddine Boudar[1] · Boubker Mehdaoui[1] · Abderrahim Aatiq[1]

Received: 1 April 2020 / Accepted: 5 May 2020 / Published online: 26 May 2020

Abstract

We report on the synthesis and structural and magnetic properties of the new $SrLa_2FeCuSbO_9$ perovskite. The compound was prepared by the solid-state reaction method. The crystalline structure was studied by X-ray diffraction experiments using the Rietveld refinement analysis. $SrLa_2FeCuSbO_9$ crystallizes in a monoclinic system ($P2_1/n$ space group). Its unit cell parameters are $a = 5.6101(2)$ Å, $b = 5.6125(2)$ Å, $c = 7.9358(3)$ Å, and $\beta = 90.094(2)°$. Sr^{2+} and La^{3+}, in $SrLa_2FeCuSbO_9$, are statistically distributed within the A-perovskite sites. The obtained cationic distribution can be illustrated by the $[SrLa_2]_A[(SbCu_{0.5})_{2c}(FeCu_{0.5})_{2d}]_BO_9$ crystallographic formula. $SrLa_2FeCuSbO_9$ was found to exhibit a paramagnetic–ferrimagnetic transition around $T_C = 215$ K. At high temperature, the magnetic susceptibility was described by the Curie–Weiss law. The experimental effective moments were explained by only spin contribution for Cu^{2+} and Fe^{3+} ions. At low temperature, the compound presents a ferrimagnetic state with signs of frustration.

Keywords Perovskite · Rietveld refinement · Cationic distribution · Magnetization · Ferrimagnetic

1 Introduction

Perovskite compounds of the general formula ABO_3, where A is an (s or f) block cation, and B is a (d or p) block cation, have been widely studied because of their very interesting and surprising physical and chemical properties [1]. These compounds represent a large percentage of systems currently studied and continue to interest scientists. In fact, it is due to the remarkable flexibility of this structure which can accommodate a wide variety of chemical elements with different oxidation states, which gives a large number of compounds with different fundamental and interesting chemical and physical properties such as electronic structures ranging from insulating to metallic [2], superconductivity [3], ferromagnetic [4], ferroelectric [5], magnetoresistance [6], and multiferroic [7]. In ABO_3 perovskite phases, if two or three different types of atoms are introduced into A and/or B sites, more complex structures, such as double perovskite $AA'BB'O_6$ and triple perovskite $A_2A'B_2B'O_9$, can be adopted [8]. In recent years, $A_3B_2B'O_9$ triple perovskites have been of great interest, because they present new promising physical properties such as relaxor ferromagnetic [9]. Recently, $SrLa_2FeCoSbO_9$ compounds have been synthesized and their structural and magnetic properties have been studied [10]. It has been found that this compound presents a relative height magnetic transition to a ferrimagnetic phase ($T_C = 215$ K). This result was related to the presence of two different magnetic (B, B') cations in the octahedral sites. Indeed, this compound adopts a monoclinic perovskite structure ($P2_1/n$ space group) with two distinct octahedral sites; one of these sites is occupied by ($2/3Co^{2+}$, $1/3Fe^{3+}$) and the other by ($2/3Sb^{5+}$, $1/3Fe^{3+}$). Similar compounds such as $La_2SrCo_2FeO_9$ [11], $La_2SrFe_2CoO_9$ [12], and $Sr_3CrFeMoO_9$ [13] have been investigated. The earlier three compounds were shown to present a ferrimagnetic state below 123 K, 280 K, and 400 K, respectively. The high magnetic transition temperature observed in these compounds seems to be linked to the presence of Fe^{3+} ions which imposes strong magnetic interactions. Several results show that the compounds which contain the same magnetic cations in two octahedral sites present a relatively low magnetic transition temperature T_C such as the

✉ Abderrahim Aatiq
a_aatiq@yahoo.fr

[1] Faculty of Sciences Ben M'Sik, Laboratory of Physical-Chemistry of Applied Materials, University Hassan II of Casablanca, Avenue Idriss El Harti, B. P. 7955, Casablanca, Morocco

compounds $La_3Ni_2SbO_9$ ($T_C = 105$ K) [9], $La_3Co_2SbO_9$ ($T_C = 55$ K) [14], $LaSr_2Cr_2SbO_9$ ($T_C = 150$ K) [15], $SrLa_2Ni_2TeO_9$ (spin glass below 35 K) [16], and $Sr_3Fe_2TeO_9$ (spin glass below 80 K) [17]. It should be noted that in this type of compounds the crystal structure, the nature of the chemical elements which are in *A*, *B*, and *B′* sites, and the cation distribution between the two *B* and *B′* sites of the perovskite structure play a determinant role on their magnetic properties. Indeed, these parameters can modulate the competition between the different types of magnetic interactions which lead to particular effects, such as magnetic frustration or high Tc ferromagnetic properties. In our previous structural characterization study, the structure of the $[CaLa_2]_A[CaTi_2]_BO_9$ phase ($P2_1/n$ space group) is shown to adopt a partial 1:1 ordering between cations in the B site whereas in the case of $[CaLn_2]_A[CuTi_2]_BO_9$ (Ln = Pr, Nd, Sm) and $[CaLn_2]_A[ZnTi_2]_BO_9$ (Ln = La, Pr, Nd, Eu) (*Pbnm* space group) the cationic distribution within the A and B sites is statistical [18–20]. In this work, we present the synthesis and structural properties of the $SrLa_2FeCuSbO_9$ compound, and their cationic distribution is obtained by using different models in the Rietveld refinement. We also present a study of the magnetic properties using magnetization measurements. The detailed relationship between the structural and magnetic properties was also investigated.

2 Experimental

The polycrystalline sample of $SrLa_2FeCuSbO_9$ was prepared by conventional solid-state reaction at high temperature from the mixture, in stoichiometric proportions, of La_2O_3, $SrCO_3$, Sb_2O_3, CuO, and Fe_2O_3 powders (purity > 99.95%). The mixture was ground, pressed, and annealed at 900 °C for 24 h, 1100 °C for 48 h, and 1200 °C for 48 h. The obtained sample is finally ground, pressed, and sintered at 1300 °C for 48 h. X-ray diffraction (XRD) experiment was performed at room temperature by means of a diffractometer Panalytical X'Pert Pro (θ-2θ) equipped with detector x'celerator radiance ($Cu_{K\alpha} = 1.5406$ Å) (45 kV, 40 mA), slope of divergence of 1°, 0.10 mm receiving slot, and anti-dispersion slot of 1°. Data were collected from 10 to 110° (2θ), in increments of 0.02°, with a count time of 15 s per step. The refinement of the crystal structure was performed by the Rietveld method [21] using the FullProf program [22]. The changes of magnetization as function of temperature (2–300 K) through zero-field cooling (ZFC) and field cooling (FC) procedures and under a fixed value of applied magnetic field of 50 Oe were performed using the Quantum Design MPMS-XL5 SQUID magnetometer. Magnetization measurements as a function of applied magnetic field (hysteresis loops) were recorded at 10 K from − 50 kOe up to + 50 kOe.

3 Results and Discussion

3.1 Structural Study

Obtained XRD pattern indicates that $SrLa_2FeCuSbO_9$ crystallizes in monoclinic symmetry ($P2_1/n$ space group). The pattern also indicates the presence of a secondary phase with a small amount (about 7% by weight) which is attributed to La_3SbO_7 (JCPDS PDF#23-1138). The structural refinements were carried out by the Rietveld method using the FullProf program. The most intense peak region due to La_3SbO_7 was excluded from the refinement. The structural model used in our refinements was based on those reported for $SrLa_2FeCoSbO_9$ ($P2_1/n$ space group) [10]. Note that in $SrLa_2FeCoSbO_9$, 1/3 of the Sr^{2+} ions and 2/3 of the La^{3+} ions are statistically distributed in the (4e) positions of *A*-perovskite sites. This structure contains two distinct (2c) and (2d) positions of the octahedral *B*-sites, which must be occupied by the smallest (Fe, Co, and Sb) elements. The oxygen ions are located in three different (4e) positions.

The first step of refinement was to determine the correct cell parameters using the $P2_1/n$ space group. In structural refinement, three models were tested and the quality of the refinements was judged based on the reliability factors (R_P, R_{wp}, R_B, R_F-factor, and Chi^2). The refined parameters were the lattice parameters, the oxygen atomic coordinates, the occupancy of the different sites, and the atomic displacement parameters of all atoms. The peak shapes were described using a pseudo-Voigt function.

The three tested models for the $SrLa_2FeCuSbO_9$ compound can be illustrated by the three crystallographic formula: $SrLa_2(CuSb_{0.5})_{2c}(FeSb_{0.5})_{2d}O_9$ in the first model (M1), $SrLa_2(CuFe_{0.5})_{2c}(SbFe_{0.5})_{2d}O_9$ in the second model (M2), and $SrLa_2(SbCu_{0.5})_{2c}(FeCu_{0.5})_{2d}O_9$ in the third model (M3). Figure 1 represents the observed and calculated shape of the

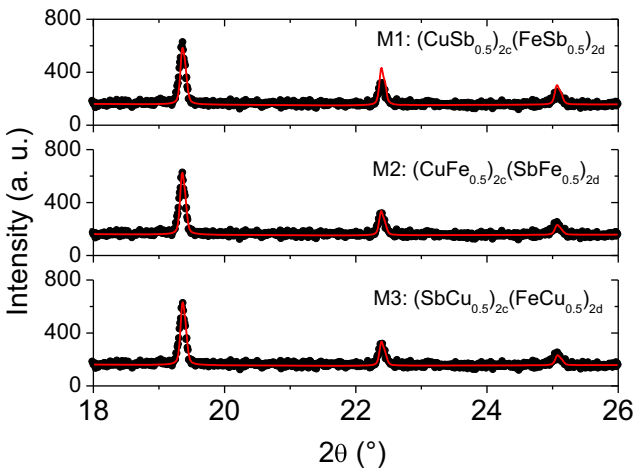

Fig. 1 Experimental (●●●) and calculated (—) XRD patterns, in the $2\theta = 18$–26° range of $SrLa_2FeCuSbO_9$, in the three models of cationic distribution

selected peak region which is more sensitive to the cationic distribution, for the three models.

The M1 model, where the Sb^{5+} ions are distributed between the two (2c) and (2d) sites, gives unsatisfactory refinement results, in good agreement with reported work for the isotypic $SrLa_2FeCoSbO_9$ compound [10]. According to obtained reliability factors, the two M2 and M3 models seem to be the best. However, for the M2 model, where the Fe^{3+} ions are distributed between the two sites, the refinement leads to negative values for the parameters of displacement of oxygen and cations in the (2c) and (2d) sites. The M3 model, where the Cu^{2+} ions are distributed between the two (2c) and (2d) sites, gives satisfactory refinement results ($R_B = 3.5\%$). Figure 2 shows the good agreement between the observed and calculated profiles obtained for the $SrLa_2(SbCu_{0.5})_{2c}(FeCu_{0.5})_{2d}O_9$ crystallographic formula. Table 1 displays details of the crystal structures, cell parameters, oxygen atomic coordinates, cationic distribution, and reliability factors.

$SrLa_2FeCuSbO_9$ adopts a crystal structure with monoclinic $P2_1/n$ space group. In this structure, 1/3 of the Sr^{2+} ions and 2/3 of the La^{3+} are statistically distributed in the A-perovskite sites. The two distinct (2c) and (2d) octahedral sites are occupied by ($2/3Sb^{5+}$, $1/3Cu^{2+}$) and ($2/3Fe^{3+}$, $1/3Cu^{2+}$), respectively. Table 2 groups the (La/Sr)–O, (Sb/Cu)–O and (Fe/Cu)–O bond distances and the different bond angles, and Fig. 3 shows the crystal structure of $SrLa_2FeCuSbO_9$. The way in which the octahedra are connected indicates that the crystal structure is typical of a perovskite with octahedral tilt distortion and that the tilt system is $a^+a^+c^-$ [23]. We also note that the angles in the $(Sb/Cu)O_6$ and $(Fe/Cu)O_6$ octahedra are all far from those of the ideal structure of perovskite. This can be explained by the tolerance factor of Goldschmidt [24]. Taking into account the ionic distribution obtained by the Rietveld refinement and based on the effective Shannon's ionic radii [25] ($r(O^{2-}) = 1.26$ Å, $r_{VI}(Cu^{2+}) = 0.87$ Å, $r_{VI}(Fe^{3+}) = 0.785$ Å, $r(La^{3+}) = 1.356$ Å, $r_{IV}(Sb^{5+}) = 0.74$ Å, $r(Sr^{2+}) = 1.45$ Å), the value of the calculated tolerance factor of Goldschmidt (t) is $t = 0.90$. This last value is low enough to give rise to significant deviations from the ideal perovskite. Note that the presence of $Cu^{2+}(3d^9)$ ions in the two (2c) and (2d) sites can reinforce the distortion of octahedra by Jahn–Teller effect, but the amount of Cu^{2+} in every B site is not in favor of their appearance. The comparison of the experimental A–O and B–O band distance values with those calculated from Shannon's ionic radii (i.e., (Sr/La)–O = 2.64 Å, (Sb/Cu)–O = 2.04 Å, and (Fe/Cu)–O = 2.09 Å) agrees well with the obtained cationic distribution (Table 2).

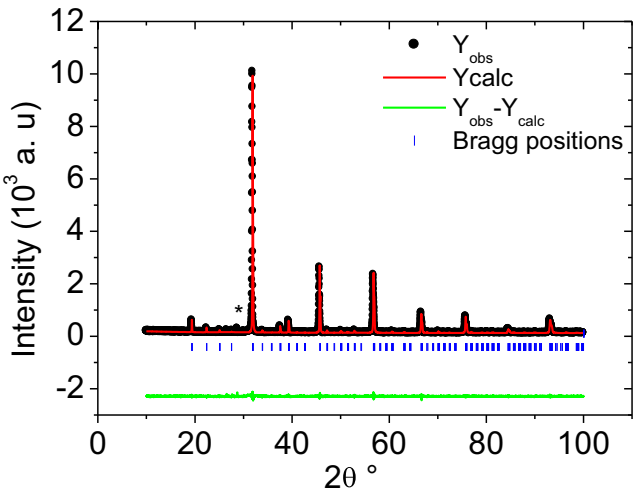

Fig. 2 Experimental (●●●), calculated (——) and difference (——) profile of the XRD pattern of $SrLa_2FeCuSbO_9$ (*La_3SbO_7)

The bond valence model [26] can give an estimate of the valences of cations and anions in a crystal structure. The value of calculated bond valence sum for each $(Sb/Cu)_{2c}$ and $(Fe/Cu)_{2d}$ sites are shown in Table 2. Note that a relativity good agreement between expected and calculated bond valence sums for the two octahedral (2c) and (2d) sites is obtained. The slight divergence observed for the (Sr/La) site, can be related to the disordered distribution of the two atom types within the same crystallographic position.

3.2 Magnetic Study

Figure 4 a shows the temperature dependence of zero field cooled (ZFC) and field cooled (FC) magnetization for $SrLa_2FeCuSbO_9$ recorded in an applied magnetic field of 50 Oe in the temperature range of (2–300) K. A clear transition from the paramagnetic to ferrimagnetic state is observed at T_C. The magnetic transition temperature T_C is extracted from the derivative dM(T)/dT (see Fig. 4b); both ZFC and FC magnetization curves show the same transition temperature $T_C = 215$ K. Fig. 5 displays the inverse magnetic susceptibility in the temperature ranges from 2 to 300 K. At high temperature ($T > T_C$), the inverse magnetic susceptibility is linear and can be described using Curie–Weiss law:

$$\chi = \frac{C}{T-\theta}$$

Here, C is the Curie constant and θ is the Curie–Weiss temperature. The results of the fit using Curie–Weiss law are plotted in Fig. 5 with a solid line. The obtained Curie constant C and Weiss constant θ are 3.81 emu K/mol and + 226 K, respectively. Experimental effective magnetic moment (μ_{eff}) was extracted from the obtained value of the Curie constant ($\mu_{eff} = 5.51\ \mu_B$/f.u). μ_{eff} was compared with the theoretical moment obtained using spin-only approximation for both Cu^{2+} and Fe^{3+} ions. The magnetic moments μ_S (Cu^{2+}) and μ_S (Fe^{3+}) can be expressed as $\mu_s(M^{n+}) = g\sqrt{S(S+1)}$, with g ($g = 2$) is the Landé factor, S (Cu^{2+}) = 1/2 and S (Fe^{3+}) = 5/2,

Table 1 Crystallographic data obtained from the Rietveld refinement for $SrLa_2CuSbFeO_9$

$[SrLa_2]_A[(SbCu_{0.5})_{2c}(FeCu_{0.5})_{2d}]_BO_9$		Monoclinic $P2_1/n$ space group				
$a = 5.6101(2)$ Å, $b = 5.6125(2)$ Å, $c = 7.9358(3)$ Å, and $\beta = 90.094(2)°$						
$R_p = 5.9\%$, $R_{wp} = 7.8\%$, $R_{exp} = 7.2\%$, $R_B = 3.5\%$, $R_F = 7.3\%$, and $chi^2 = 1.1\%$						
Atom	Site (w.p.)	x	y	z	B_{iso} (Å^2)	Occupancy
Sr	4e	0.500(1)	0.520(3)	0.250(1)	1.167(5)	1/3
La	4e	0.500(1)	0.520(3)	0.250(1)	1.167(5)	2/3
Sb	2c	0.0	0.5	0.0	0.183(5)	2/3
Cu(1)	2c	0.0	0.5	0.0	0.183(5)	1/3
Fe	2d	0.5	0.0	0.0	0.183(5)	2/3
Cu(2)	2d	0.5	0.0	0.0	0.183(5)	1/3
O(1)	4e	0.283(8)	0.306(7)	0.012(5)	0.10(1)	1
O(2)	4e	0.229(6)	0.769(5)	0.059(5)	0.10(1)	1
O(3)	4e	0.544(9)	1.006(2)	0.243(5)	0.10(1)	1

which give μ_S (Cu^{2+}) = 1.73 μ_B and μ_S (Fe^{3+}) = 5.91 μ_B. The total theoretical moment was calculated using the following formula: $\mu_{theo} = \sqrt{\mu_s^2(Cu^{2+}) + \mu_s^2(Fe^{3+})}$ (μ_B/formula unit), the obtained theoretical moment is $\mu_{theo} = 6.15$ μ_B, which is slightly higher than the experimental one ($\mu_{eff} = 5.51$ μ_B) with a difference $\Delta\mu = |\mu_{eff}\text{-}\mu_{theo}|$ of 10.4%. This difference could be attributed to the presence of impurities (La_3SbO_7) detectable by XRD. On the other hand, the Curie–Weiss temperature value ($\theta = +226$ K) is high and positive which indicates the dominance of strong ferromagnetic interactions at low temperature. In addition, the transition temperature $T_C = 215$ K is very close to the Curie–Weiss temperature θ with a ratio of $f = \theta/T_C = 1.05$. This obtained value of the f parameter is characteristic of a ferromagnetic behavior [27]. At low temperature ($T < T_C$), the magnetization curves ZFC and FC increase rapidly and stabilize at low temperature (see Fig. 4a), indicating the establishment of a ferrimagnetic order. The magnetization curves ZFC and FC show the existence of irreversibility over a wide temperature range ($T < T_C$). A similar difference in ZFC and FC magnetization data has been reported in disordered double and triple perovskite compounds $La_3Ni_{2-x}Cu_xB'O_9$ (B' = Sb, Ta, Nb) [28], La_2BMnO_6 (B =

Table 2 Bond lengths (Å), bond angles (°), and bond valence sum (BVS) for $SrLa_2FeCuSbO_9$

Bonds	Length (Å)	BVS	Angles (°)	
(La/Sr)-O(1)	2.54 (4)	0.35	O1-(Cu/Sb)–O(2)	83(3) × 2
(La/Sr)-O(1)	2.93 (4)	0.12	O1-(Cu/Sb)–O(2)	97(3) × 2
(La/Sr)-O(1)	2.61 (4)	0.29	O1-(Cu/Sb)–O(3)	93(3) × 2
(La/Sr)-O(2)	2.55 (3)	0.34	O1-(Cu/Sb)–O(3)	87(3) × 2
(La/Sr-O(2)	2.43 (3)	0.47	O2-(Cu/Sb)–O(3)	80(3) × 2
(La/Sr)-O(2)	3.01 (4)	0.09	O2-(Cu/Sb/)–O(3)	100(3) × 2
(La/Sr)-O(3)	2.89 (1)	0.14	O1-(Cu/Fe)–O(2)	94(3) × 2
(La/Sr)-O(3)	2.74 (1)	0.20	O1-(Cu/Fe)–O(2)	86(3) × 2
(La/Sr)-O(3)	2.55 (5)	0.34	O1-(Cu/Fe)–O(3)	90(3) × 4
Bond valence sum (La/Sr-site) = 2.34 (should be 2.66)			O1-(Cu/Fe)–O(3)	83(3) × 2
(Cu/Sb)–O(1)	2 × 1.92(4)	0.84 × 2	O(2)-(Cu/Fe)–O(3)	97(3) × 2
(Cu/Sb)–O(2)	2 × 2.04(3)	0.60 × 2	(Cu/Sb)–O(1)-(Cu/Fe)	158.7(1) × 2
(Cu/Sb)–O(3)	2 × 2.05(4)	0.59 × 2	(Cu/Sb)–O(2)–(Cu/Fe)	151.6(1) × 2
Bond valence sum (Cu/Sb-site) = 4.06 (should be 4.00)			(Cu/Sb)–O(3)–(Cu/Fe)	165.9(1) × 2
(Cu/Fe)–O(1)	2 × 2.10(4)	0.37 × 2		
(Cu//Fe)–O(2)	2 × 2.05(3)	0.42 × 2		
(Cu/Fe)–O(2)	2 × 1.94(4)	0.57 × 2		
Bond valence sum (Cu/Fe-site) = 2.72 (should be 2.66)				

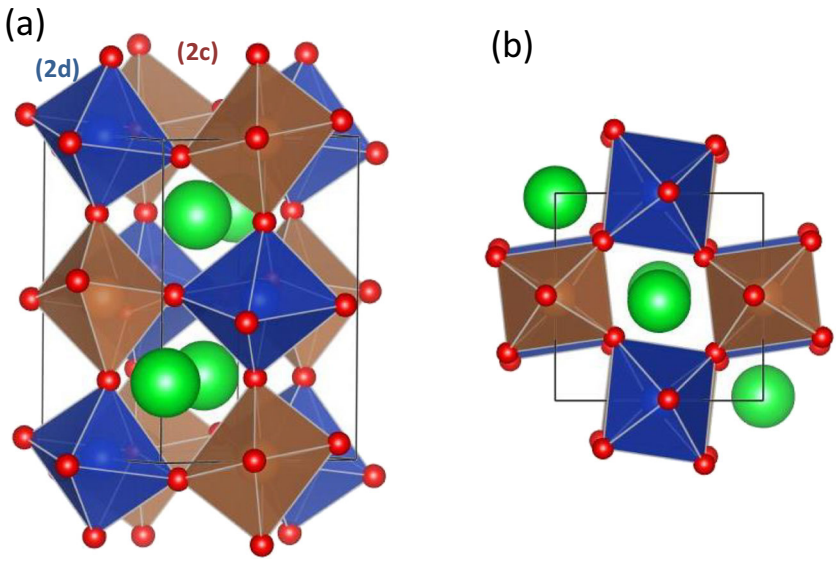

Fig. 3 Crystal structure of $SrLa_2FeCuSbO_9$. **a** Cell in perspective. **b** Cell projected in (001) direction, putting to see the structure of the tilt system ($a^+a^+c^-$). Sr^{2+} and La^{3+} in the *A* site are represented by a circle in green

Ni or Co) [29]. This behavior has been explained by a disordered magnetic system such as spin glasses and clusters glasses [9, 12].

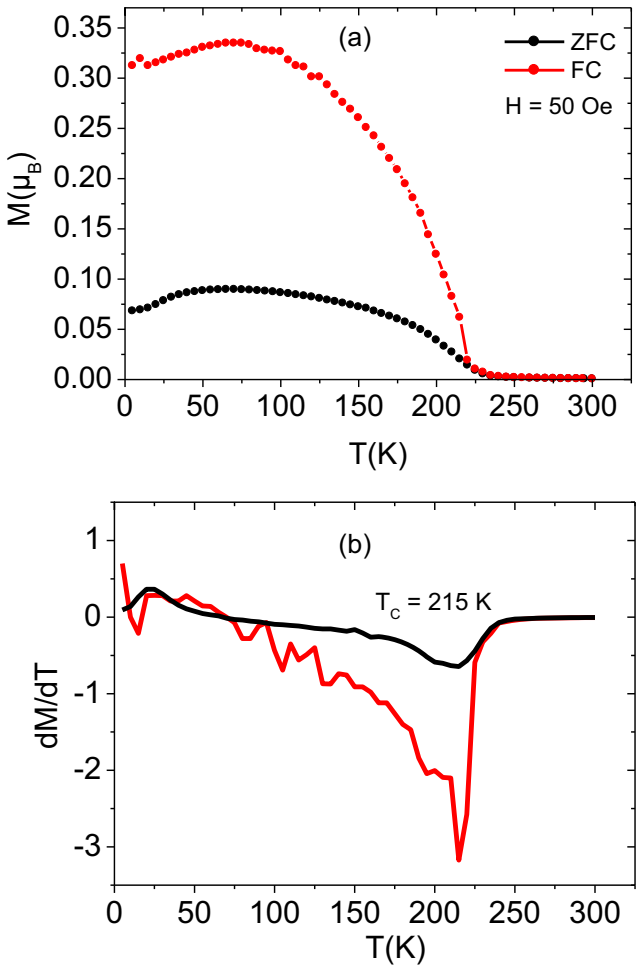

Fig. 4 **a** ZFC/FC magnetization as a function of temperature. **b** Evolution of the derivative magnetization with respect to temperature

Figure 6 displays the magnetization as a function of the applied magnetic field at 10 K. The magnetization curve shows a weak hysteresis loop typical of a ferrimagnetic system with an unsaturated character up to 50 kOe, weak coercive field ($H_C = 195$ Oe) and remanent magnetization $M_r = 0.45\ \mu_B$/f.u. (see inset in Fig. 6). The first magnetization as a function of the magnetic field shows a rapid increase for low magnetic fields, followed by a linear increase as a function of the applied magnetic field without saturation, which indicates blocked magnetic moments due to the inhomogeneity in the distribution of magnetic moments caused by cationic disorder. The spontaneous magnetization M_s was deduced by extrapolating to $H = 0$ Oe the linear part of the magnetization curve; M_s is found to be close to 1.46 μ_B/f.u.

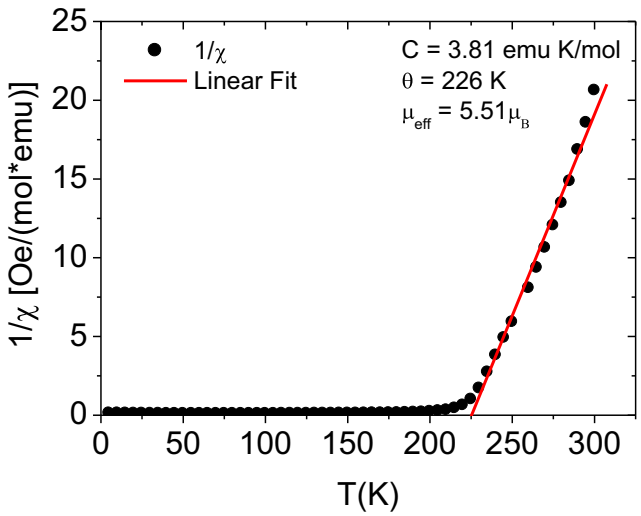

Fig. 5 Inverse of magnetic susceptibility χ^{-1} as a function of temperature recorded under a magnetic field of 50 Oe. The red line shows the Curie–Weiss fit at high temperatures

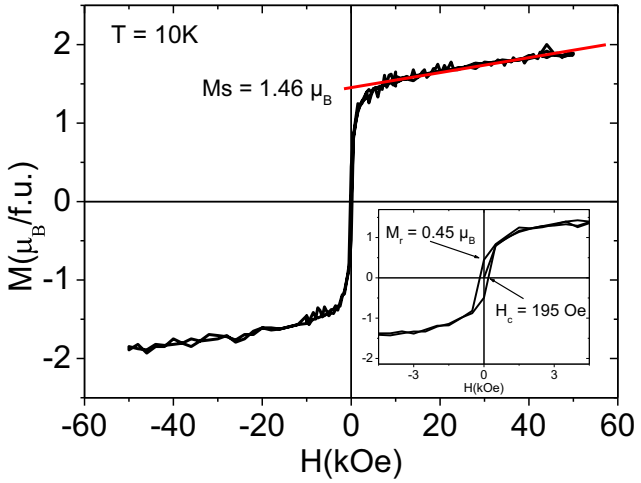

Fig. 6 Magnetization curves as a function of magnetic field up to 50 kOe recorded at a temperature of 10 K. Inset: zoom in the range of the magnetic field between − 3.5 kOe and + 3.5 kOe

It is of interest to note that the M_r/M_s ratio can give an idea on the structure of magnetic domains in ferromagnetic or ferrimagnetic materials. As well, it is known that for polycrystalline samples with uniaxial and cubic magnetocrystalline anisotropy, the M_r/M_s ratios are 0.50 and 0.83, respectively [30, 31]. Furthermore, the M_r/M_s ratio equal to or greater than 0.5 indicates that the sample can be in the form of nanoparticles with a single magnetic domain, and for M_r/M_s less than 0.5 it indicates the formation of a multidomain structure [32, 33]. In our case, the calculated M_r/M_s ratio, at $T = 10$ K, is approximately 0.30. This last value is less than 0.50, which could indicate the formation of a multidomain structure, in accordance with the structure of our compound as a bulk material. Otherwise, this low value of M_r/M_s can also be related to the inhomogeneity in the distribution of magnetic moments caused by the cationic disorder.

Assuming a G-type collinear ferrimagnetic arrangement, where Fe^{3+}(S = 5/2), Cu^{2+}(S = 1/2), and Sb^{5+} (diamagnetic) ions are distributed in a disordered manner in the two different (2c) and (2d) crystallographic sites, the spontaneous magnetization M_s can be estimated by the Néel model assuming a mean magnetization in each site. Considering the cationic distribution formula, the mean values of magnetizations M(2c) in the (2c) and M(2d) in the (2d) sites are 3.66 μ_B and 0.33 μ_B, respectively. Therefore, the net magnetization M_s can be calculated by the Néel model $M_s = M(2c) - M(2d)$. The magnitude of the net magnetization M_s per formula unit should be 3.33 μ_B/f.u. However, the experimental value of 1.46 μ_B/f.u. is considerably less than the theoretical value, which indicates that the compound is far from saturated. This behavior has already been observed on triple-perovskite compounds [9, 15, 34, 35] which might be attributed to the following reasons. First, the cationic disorder imposed by non-magnetic ions such as Sb^{5+} ions disrupts the magnetic interactions, which prevents the establishment of a long-range magnetic order and leads to the formation of magnetic domains. Therefore, the low magnetization measured at low temperature is attributed to the spontaneous magnetization present in each domain. This behavior was observed on the partially disordered $La_3Ni_2SbO_9$ compound, which behaves as a ferrimagnetic relaxant below 110 K [9]. Secondly, the weak magnetization measured at low temperature is linked to the weakening of the efficiency and the dominance of the magnetic NN interactions by the presence of the diamagnetic Sb^{5+} ions. NN interactions are magnetic superexchange intercations between the nearest neighboring cations [10]. In this case, the long-range magnetic order is maintained, but the NN coupling is weakened. This is the case for the $SrLa_2FeCoSbO_9$ compound which has a magnetic transition temperature ($T_C = 215$ K) higher than that of $La_3Ni_2SbO_9$ [9, 10].

This second model seems to give an explanation of the magnetic behavior observed at low temperature in our compound which presents a cationic disorder with a relative high transition temperature ($T_C = 215$ K) similar to that observed for $SrLa_2FeCoSbO_9$. The positive Curie–Weiss temperature $\theta = +229$ K, the shape of the ZFC/FC magnetization curves and the presence of a hysteresis loop are characteristic of a ferromagnetic behavior. However, the existence of a high irreversibility at low temperatures between the ZFC and FC magnetization curves and the low value of the spontaneous magnetization at $H = 50$ kOe indicates the presence of inhomogeneity in magnetic interactions caused by the cationic disorder. In order to improve the understanding of the magnetic interactions in this compound, neutron diffraction and electronic microscopy will be useful.

4 Conclusion

In summary, we have investigated the structural and magnetic properties of $SrLa_2FeCuSbO_9$. The crystal structure was refined by X-ray powder diffraction data in the monoclinic $P2_1/n$ space group. The *A* sites are statistically occupied by 1/3 of Sr^{2+} ions and 2/3 of La^{3+}. The two distinct octahedral (2c) and (2d) sites are occupied by (2/3Sb^{5+}, 1/3Cu^{2+}) and (2/3Fe^{3+}, 1/3Cu^{2+}), respectively. The result of the structural analysis indicates that the crystal structure of our compound is typical of a perovskite with octahedral tilt distortion and that the tilt system is $a^+a^+c^-$. Magnetization measurements indicate a paramagnetic–ferrimagnetic transition around $T_C = 215$ K. In the paramagnetic region, the magnetic susceptibility was described by Curie–Weiss law. The experimental effective moments were explained by only spin contribution for the Fe^{3+} and Cu^{2+} ions. The effective magnetic moment obtained experimentally is $\mu_{eff} = 5.51$ μ_B/f.u. The positive and high Curie–Weiss temperature ($\theta = +226$ K) indicates the dominance of strong ferromagnetic interactions at low temperature. The obtained value of the frustration parameter is

characteristic of a ferromagnetic behavior. In the ordered magnetic regime, the shape of the ZFC/FC magnetization curves and the presence of a hysteresis loop are characteristic of a ferrimagnetic behavior. However, the existence of a high irreversibility at low temperatures between the ZFC and FC magnetization curves and the low value of the spontaneous magnetization at $H = 50$ kOe indicates the presence of inhomogeneity in magnetic interactions caused by the cationic disorder. Finally, these results will be useful to understand the magnetic properties in $SrLa_2FeCuSbO_9$.

Funding Information This study was financially supported by the Moroccan Ministry of Higher Education, Scientific Research and Training (MESRSFC) managerial staff, National Center for Scientific and Technical Research (CNRST).

Compliance with Ethical Standards

Conflict of Interest The authors declare that they have no conflict of interest.

References

1. Tilley, R.J.: Perovskites: structure-property relationships. John Wiley & Sons, New York (2016)
2. Torrance, J., Lacorre, P., Nazzal, A., Ansaldo, E., Niedermeyer, C.: Systematic study of insulator-metal transitions in perovskites $RNiO_3$ (R= Pr, Nd, Sm, Eu) due to closing of charge-transfer gap. Phys. Rev. B. **45**, 8209 (1992)
3. Maeno, Y., Hashimoto, H., Yoshida, K., Nishizaki, S., Fujita, T., Bednorz, J., Lichtenberg, F.: Superconductivity in a layered perovskite without copper. Nature. **372**, 532 (1994)
4. Park, J.H., Vescovo, E., Kim, H.J., Kwon, C., Ramesh, R., Venkatesan, T.: Direct evidence for a half-metallic ferromagnet. Nature. **392**, 794–796 (1998)
5. Ronald, E.C.: Origin of ferroelectricity in perovskite oxides. Nature. **358**, 136–138 (1992)
6. Kobayashi, K.I., Kimura, T., Sawada, H., Terakura, K., Tokura, Y.: Room-temperature magnetoresistance in an oxide material with an ordered double-perovskite structure. Nature. **395**, 677–680 (1998)
7. Fernandez-Posada, C.M., Castro, A., Kiat, J.-M., Porcher, F., Pena, O., Alguero, M., Amorin, H.: A novel perovskite oxide chemically designed to show multiferroic phase boundary with room-temperature magnetoelectricity. Nat. Commun. **7**, 12772 (2016)
8. Anderson, M.T., Greenwood, K.B., Taylor, G.A., Poeppelmeier, K.R.: B-cation arrangements in double perovskites. Prog. Solid State Chem. **22**, 197–233 (1993)
9. Battle, P.D., Evers, S.I., Hunter, E.C., Westwood, M.: $La_3Ni_2SbO_9$: a relaxor ferromagnet. Inorg. Chem. **52**, 6648 (2013)
10. Tang, Y., Hunter, E.C., Battle, P.D., Hendrickx, M., Hadermann, J., Cadogan, J.M.: Ferrimagnetism as a consequence of unusual cation ordering in the perovskite $SrLa_2FeCoSbO_9$. Inorg. Chem. **57**, 7438 (2018)
11. Albornoz, J.C., Landínez Téllez, D.A., Roa-Rojas, J., Munévar, J.A., Baggio-Saitovich, E.: Structural and magnetic properties of the new $La_2SrCo_2FeO_9$ triple perovskite. J. Supercond. Nov. Magn. **26**, 2313–2317 (2012)
12. Casallas, F., Vera, E., Landínez, D., Parra, C., Roa, J.: Structural properties, electric response and magnetic behaviour of $La_2SrFe_2CoO_9$ triple complex perovskite. Phys.: Conf. Ser. **687**, 012047 (2016)
13. Li, Z., Jiao, L., Ji, W.J., Xu, J., Wang, J.F., Gu, Z.B., Zhou, J., Yao, S.-H., Chen, Y.B., Zhang, S.-T.: Yan-Feng: triple perovskite $Sr_3CrFeMoO_9$ ultrathin films with ferromagnetism above room temperature. Scr. Mater. **69**, 590 (2013)
14. Franco, D.G., Fuertes, V.C., Blanco, M.C., Fernandez-Diaz, M.T., Sanchez, R.D., Carbonio, R.E.: Synthesis, structure and magnetic properties of $La_3Co_2SbO_9$: a double perovskite with competing antiferromagnetic and ferromagnetic interactions. J. Solid State Chem. **194**, 385–391 (2012)
15. Hunter, E.C., Battle, P.D., Paria Sena, R., Hadermann, J.: Ferrimagnetism as a consequence of cation ordering in the perovskite $LaSr_2Cr_2SbO_9$. J. Solid State Chem. **248**, 96–103 (2017)
16. Paria Sena, R., Hadermann, J., Chin, C.M., Hunter, E.C., Battle, P.D.: Structural chemistry and magnetic properties of the perovskite $SrLa_2Ni_2TeO_9$. J. Solid State Chem. **243**, 304–331 (2016)
17. Tang, Y., Hunter, E.C., Battle, P.D., Paria Sena, R., Hadermann, J., Avdeev, M., Cadogan, J.M.: Structural chemistry and magnetic properties of the perovskite $Sr_3Fe_2TeO_9$. J. Solid State Chem. **242**, 86–95 (2016)
18. Aatiq, A.: Crystal structure of the new perovskite $CaLa_2CaTi_2O_9$(=$(Ca_{1/3}La_{2/3})_A$ $(Ca_{1/3}Ti_{2/3})_BO_3$). Solid State Sci. **5**, 745–749 (2003)
19. Aatiq, A., Boukhari, A.: Synthesis and structural study of the new perovskite series $CaLn_2ZnTi_2O_9$(= $(Ca_{1/3}Ln_{2/3})_A$ $(Zn_{1/3}Ti_{2/3})_BO_3$) (Ln = La, Pr, Nd, Eu). Mater. Lett. **58**, 2406–2411 (2004)
20. Iturbe-Zabalo, E., Igartua, J.M., Aatiq, A., Pomjakushin, V.: A structural study of the $CaLn_2CuTi_2O_9$ (Ln = Pr, Nd, Sm) and $BaLn_2CuTi_2O_9$ (Ln = La, Pr, Nd) triple perovskite series. J. Mol. Struct. **25**, 205–401 (2013)
21. Rietveld, H.M.: A profile refinement method for nuclear and magnetic structures. J. Appl. Crystallogr. **2**, 65–71 (1969)
22. Rodriguez-Carvajal, J.: Recent advances in magnetic structure determination by neutron powder diffraction. Phys. B Condens. Matter. **192**, 55–69 (1993)
23. Woodward, P.M.: Octahedral tilting in perovskites. I. Geometrical Considerations. Acta Cryst. B. **53**, 32–43 (1997)
24. Goldschmidt, V.M.: Die Gesetze der Krystallochemie. Naturwissenschaften. **14**, 477–485 (1926)
25. Shannon, R.D.: Revised effective ionic radii and systematic studies of interatomic distances in halides and chalcogenides. Acta Crystallogr. A. **32**, 751–767 (1976)
26. Brown, I.D., Altermatt, D.: Bond-valence parameters obtained from a systematic analysis of the Inorganic Crystal Structure Database. Acta Crystallogr. B. **41**, 244–247 (1985)
27. Ramirez, A.P.: Strongly geometrically frustrated magnets. Annu. Rev. Matter. Sci. **24**, 453–480 (1994)
28. Chin, C.M., Battle, P.D., Hunter, E.C., Avdeev, M., Hendrickx, M., Hadermann, J.: Stabilisation of magnetic ordering in $La_3Ni_{2-x}Cu_xB'O_9$ (B' = Sb, Ta, Nb) by the introduction of Cu^{2+}. J. Solid State Chem. **276**, 164–172 (2019)
29. Mao, Y., Parsons, J., McCloy, J.S.: Magnetic properties of double perovskite La_2BMnO_6 (B = Ni or Co) nanoparticles. Nanoscale. **5**, 4720 (2013)
30. Chikazumi, S., Graham Jr., C.D.: Physics of ferromagnetism. Oxford Clarendon Press, Oxford (1997)
31. Xie, X., Che, H., Wang, H., Lin, G., Zhu, H.: Negative zero-field-cooled magnetization in $YMn_{0.5}Cr_{0.5}O_3$ due to giant coercivity and trapped field. Inorg. Chem. **57**, 175–180 (2018)
32. Ali, I., Islam, M.U., Awan, M.S., Ahmad, M., Ashiq, M.N., Naseem, S.: Effect of Tb^{3+} substitution on the structural and magnetic properties of M-type hexaferrites synthesized by sol–gel autocombustion technique. J. Alloy. Compd. **550**, 564–572 (2013)
33. Almessiere, M.A., Slimani, Y., Sertkol, M., Nawaz, M., Sadaqat, A., Baykal, A., Ercan, I., Ozçelik, B.: Effect of Nb^{3+} substitution on

the structural, magnetic, and optical properties of $Co_{0.5}Ni_{0.5}Fe_2O_4$ nanoparticles. Nanomaterials. **9**, 430 (2019)

34. Tang, Y., Paria Sena, R., Avdeev, M., Battle, P.D., Cadogan, J.M., Hadermann, J., Hunter, E.C.: Magnetic properties of the 6H perovskite $Ba_3Fe_2TeO_9$. J. Solid State Chem. **253**, 347–354 (2017)
35. Wang, J.F., Hu, B., Zhang, J., Gu, Z.B., Zhang, S.T.: Composition dependent magnetism in novel triple perovskite $Sr_3MFeMoO_9$ (M=Mn, Co, Ni). Ceram. Int. **40**, 8753–8759 (2014)